AJNR

Newer Sequences for Spinal MR Imaging: Smorgasbord or Succotash of Acronyms?

Jeffrey S. Ross

AJNR Am J Neuroradiol 1999, 20 (3) 361-373
http://www.ajnr.org/content/20/3/361

AJNR Am J Neuroradiol 20:361–373, March 1999

Review Article

Newer Sequences for Spinal MR Imaging: Smorgasbord or Succotash of Acronyms?

Jeffrey S. Ross

With the tremendous technical advances in MR imaging of the brain, such as perfusion, diffusion, and blood oxygenation level-dependent (BOLD) functional imaging, and contrast-enhanced MR angiography, the continued advances in MR imaging of the spine unfortunately may be overlooked. Nevertheless, despite being somewhat overshadowed by their flashier cephalad cousins, significant advances have been made in sequence design and implementation that will directly impact the ease and confidence of spinal disease interpretation.

In the performance of any MR examination, major decisions include selection of the appropriate coil, imaging plane, slice thickness, imaging matrix, number of excitations, and pulse-sequence parameters. These choices will be influenced by the anatomic area to be studied, the desired field of view (FOV), spatial resolution, and contrast needs. The goal is to provide a voxel size that provides adequate yet small enough signal-to-noise (S/N) ratios for contrast resolution that provide the necessary spatial resolution. From a minimalist standpoint, what is desired is enough contrast to noise (C/N) in the shortest imaging time to provide diagnostic accuracy. This should be in a form that is quick and easy to interpret, and eliminates tedious multiple imaging manipulation and off-line processing.

Many novel MR imaging techniques have been developed with one of two driving forces behind them—increased speed of acquisition or improved lesion detection. Fortunately, a convergence of these forces has also occurred, allowing for current sequences with high C/N and short examination times.

A myriad of choices are available for spine imaging, often with a bewildering array of names, acronyms, and parameters. Even more choices are potentially available, but have shown little clinical use. This review will focus on some new sequences that might have real clinical impact on spinal imaging, as well as new applications of some older techniques. First, a few disclaimers: this review is necessarily limited, and I do not presume to cover every conceivable pulse sequence. Cord and CSF motion studies will not be covered, and peripheral nerve evaluations such as the lumbar and cervical plexi have been reviewed recently (1, 2). Second, the majority of sequences discussed were obtained at mid and high field (1–1.5 T); therefore, I cannot attest to their usefulness at lower field strength. Thirdly, and as is often the case with rapidly changing technology, the sequences may be quickly put into clinical use without much support in the scientific literature. Existing literature tends to be preliminary, and reports findings in few patients. No apologies are offered for potentially sending the interested and highly motivated reader down an ultimately useless sequence road.

Received in original form September 14, 1998; accepted after revision November 5, 1998.

From the Department of Radiology, Cleveland Clinic Foundation, Cleveland, OH.

Address reprint requests to Jeffrey S. Ross, Division of Radiology, Magnetic Resonance, Desk L-10, Cleveland Clinic Foundation, 9500 Euclid Ave., Cleveland, OH, 44195.

Techniques

A brief overview of gradient echo (GE), fast spin echo (FSE), and diffusion sequences follows, with the clinical applications of various newer sequences provided in the second portion.

Gradient Echo

Gradient echo (GE) imaging does not use a 180° pulse to achieve the echo. This gradient-driven echo allows for rapid imaging with very short repetition time (TR). Intrinsic to good image quality in GE imaging is the choice of flip angle, which has optimal values for specific TRs and tissue types, the Ernst angle (the longer the T1 of the tissue, the smaller the best flip angle). There are two types of GE imaging; spoiled and steady-state. Spoiled sequences (fast low-angle shot [FLASH] and spoiled gradient-recalled acquisition in steady state [GRASS]) destroy the residual transverse magnetization after each alpha pulse. In steady-state sequences (fast-imaging steady precession [FISP], steady-state free precession [SSFP], and GRASS), this transverse magnetization is maintained and stabilizes after a few pulses. For tissue with a short T2 (e.g., fat, muscle), or sequences requiring long TR, the spoiled and steady-state sequences look the same. If the T2 of interest is long (e.g., CSF), then the steady-state sequence will give the familiar CSF myelogram effect. Flip angle is a powerful modifier of GE contrast. Spoiled GE sequences will be more T1-weighted with higher flip angles approaching 90°. For steady-state sequences where the TR is shorter than the T2, tissues with long T1 and T2 will show preferentially increased signal with increasing flip angle. Spin-density images can be obtained with a GE technique with short TR if a small flip angle is used. T2-like contrast (T2*) can be obtained with increasing echo time (TE), as with conventional SE imaging.

Fast Spin Echo (FSE)

The next branch on an evolving tree of fast imaging is rapid acquisition relaxation enhancement (RARE). In conventional SE techniques, one Ky line (phase-encoding line) is obtained for each 90–180° pulse pair. A 256 x 256 matrix would require 256 such pulses. FSE techniques are based on a modification of the original RARE techniques. FSE acquires all Ky lines after one 90° pulse, with the number of 180° pulses equal to the total number of Ky lines. If some portions (or segments) of all the Ky lines are obtained after a 90° pulse by using multiple 180° pulses, then the sequence is hybrid RARE, also called FSE, or turbo SE. Many excellent reviews of FSE are available (3–5). Three-dimensional (3D) versions of FSE are available, but have not been widely used in spinal imaging (6–8).

In routine SE imaging, the image contrast is controlled by the TR and the TE. New parameters were added with FSE, such as echo train length (ETL) and echo spacing, that can be manipulated to alter image contrast. New artifacts and appearances are also added by these techniques, such as T2 filtering (image blurring), bright fat, and diminished sensitivity to susceptibility effects. Because multiple echos are obtained at different TEs in the FSE sequence, the overall image has not one *true* TE, but an *effective* TE. What then determines the image appearance? A fundamental concept necessary to grasp the power and sophistication of these sequences is k-space. The method by which k-space is sampled will determine the appearance and artifacts of the final image. Think of k-space as a ''box'' that must be filled with data to get an image, and this box initially exists in the time domain. The Fourier transform takes this time domain data and converts it to the spatial domain; the image that we view. Where the data is in the k-space box determines image contrast. The central aspect of the box (low spatial frequencies) determines image contrast. These low spatial frequencies are generated with the low-amplitude phase-encoding gradients. The peripheral portions of k-space determine resolution (high spatial frequencies). These are generated with the higher amplitude phase-encoding gradients. The overall appearance of the image is heavily weighted by the relatively small amount of data collected from central k-space. In the example above, if the low spatial frequencies are collected around 80 ms, then that is the effective TE.

Longer echo trains and shorter echo spacing have been shown to improve CSF/disk contrast and cord differentiation. This is in part related to the multiple 180° refocusing pulses that minimize CSF motion effects, and the edge enhancement that occurs with collection of the low spatial frequencies late in the echo train (5–9). The temptation to have a long-echo train for the tremendous time it saves must be weighed against the disadvantages of increased T2 decay that blurs images, and a heavily T2-weighted sequence that may decrease lesion contrast (10). Frequency-selective fat saturation may be added to the FSE sequence to diminish the annoyance of the high-signal-intensity fat and chemical shift artifact. The benefit of the fat-saturation pulse will decrease as the TE is lengthened; the fat signal will diminish regardless. On the downside, the fat-saturation pulse will slightly increase the energy deposited within the patient. Also, because of the time necessary to implement the fat-saturation pulse, the sequence time is necessarily increased. Sequence time may be kept constant by collecting a decreased number of slices.

Diffusion

MR diffusion-weighted imaging (DWI) reveals the random molecular motion of water (Brownian motion), and was defined as intravoxel incoherent motion by Le Bihan et al (11–13). In biological systems, free diffusion is restricted by physical barriers (cell membranes) and chemical interactions, and is anisotropic. Differences in restricted diffusion-to-water proportions give information about the physical and physiologic state of the brain and the spinal cord. The major principle of the DWI pulse sequence is the addition of a pair of diffusion-sensitized gradient pulses to a standard MR sequence (Fig 1).

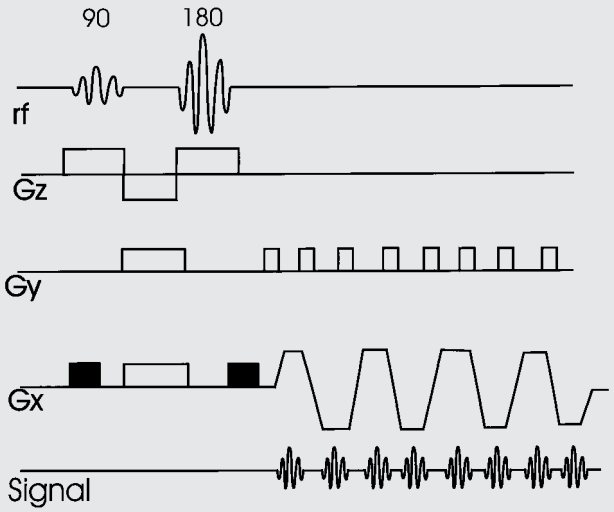

FIG 1. EPI diffusion-sequence structure. The 90° and 180° RF pulses are followed by a bipolar, trapezoidal frequency encode gradient (*Gx*) for rapid collection of multiple echos. DWI is applied by symmetrical gradients along a frequency-encoded direction (*black rectangles*). Subsequent sequence acquisitions would apply diffusion weighting along phase (*Gy*) and slice-select (*Gz*) directions.

This causes dephasing of spins (signal loss) of water that is rapidly diffusing along the direction of the applied gradient. Normal diffusion of water, therefore, results in signal loss, and diminished or restricted diffusion occurring in pathologic states results in increased signal on the raw images. Apparent diffusion coefficient (ADC) maps are plotted by images generated from sequences repeated with higher diffusion gradients. On the ADC maps, faster diffusion is increased in signal, and slowed diffusion is lower in signal.

Half Fourier and Data Synthesis

Many relatively routine pre- and postprocessing imaging techniques have been tailored for the commercial user to allow straightforward applications. One simple example would be obtaining interleaved slices as two separate sequences strung together. A similar example is the three-dimensional constructive interference in steady state (3D CISS) sequence where the two phase-alternated sequences are merged together to reduce banding artifacts. It behooves the imager to recognize these types of manipulations, as they may take the data one more step from the actual condition of the patient, and may introduce new artifacts or appearances. Other techniques are available, and may be just a click of the mouse away on the image setup screen. These techniques either synthesize, share, or create data. A common example among these latter techniques is half Fourier and interpolation.

Half Fourier should really be called ''slightly more than half Fourier''; the technique uses all the negative phase-encoded data, and the lowest amplitude positive phase-encoded data to fill the image matrix (Fig 2). The high-amplitude positive data is synthesized from the negative data. This technique works because the raw data is symmetrical (Hermitian symmetry). Because only a portion of the Ky lines are being collected in real time, this technique can dramatically reduce imaging times, particularly when applied with FSE. One sequence used to reduce the artifacts from spinal metal implants uses an FSE technique with half Fourier (HASTE) (14, 15). Half Fourier has also been used to reduce scan time in 3D FSE acquisitions for brain applications, but has not been applied to the spine (16).

Another manipulation technique that has much wider applications for sequences beyond the spine is interpolation, also very appropriately called ''zero fill'' (17). This technique cre-

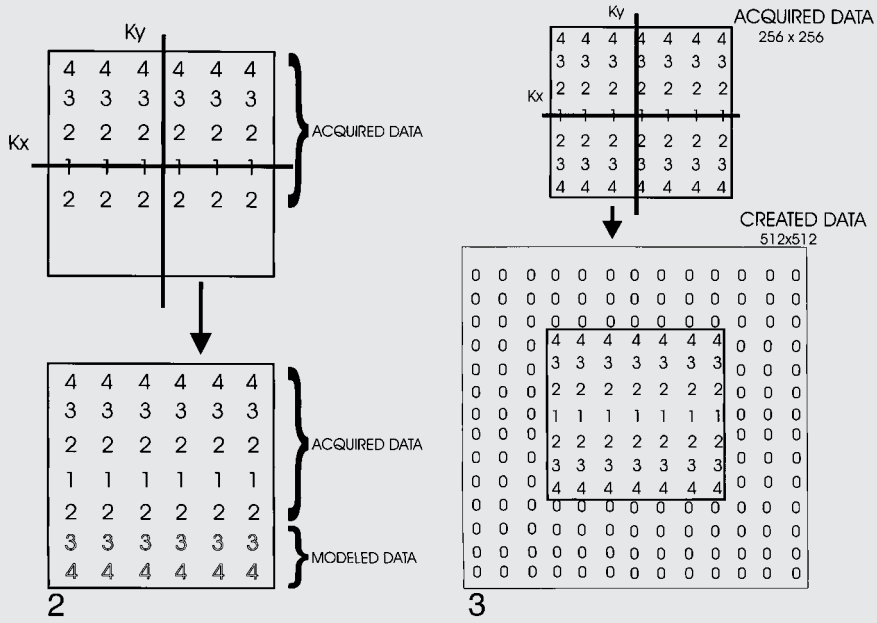

FIG 2. Half Fourier schematic. Slightly more than half of the data can be collected and used to "fill in" the remainder of k-space because the data is assumed to be symmetrical. This partial data acquisition shortens imaging time.

FIG 3. Interpolation schematic. Matrix is expanded by addition of "place holder" data, allowing reconstruction, for example, of a 512 matrix from a 256 data set. Appearance of image will be filtered due to more heavy weighting from central k-space data.

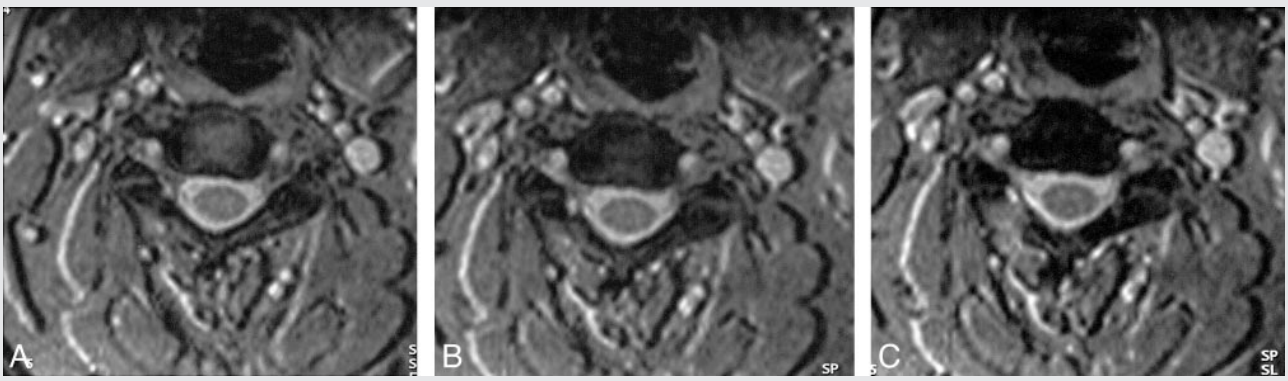

FIG 4. 3D GE with slice interpolation (36/15/1). Three contiguous slices reconstructed at 1.5 mm and acquired at 3 mm with slice interpolation. The advantage is that neural foramina are encompassed by multiple images with very-thin-slice reconstruction.

ates data to fill out the imaging matrix, using the image contrast that is primarily in central k-space to best advantage. Because image contrast is so dependent upon the central k-space data, adding data (zeros) to the periphery of k-space allows reconstruction of a 512 x 512 matrix with the time of a 256 x 256 acquisition while maintaining the overall image contrast (Fig 3). A similar technique can be used in the slice-select direction to decrease slice thickness (Fig 4). Nothing is free, so this technique does introduce a low-pass filter effect due to the weighting of real data from central k-space. The more one attempts to improve resolution with this technique without increasing imaging time, the more filtered the final image becomes.

Spinal Cord Abnormalities

FSE, blemishes and all, has become the de facto gold standard for spinal sagittal T2 and spin-density weighted imaging (18–22). The axial plain is considerably more challenging. My current choice for routine intra- and extradural disease for the cervical spine is an axial 3D low-flip angle GE sequence, reserving the two-dimensional (2D) GE sequence for patients with too much motion artifact on the 3D sequence. We do not routinely use a 3D T2-weighted FSE sequence for cervical degenerative disease. For the thoracic spine, an axial 2D GE sequence is acceptable. FSE techniques are more difficult to use in the cervical and thoracic spine because of CSF pulsation artifacts. In the lumbar spine, an axial T2-weighted FSE sequence is optimal because CSF pulsation artifact is not a significant problem. Because T2-weighted FSE is a standard technique, it will not be discussed other than in comparison to the newer sequences.

Fast Fluid-Attenuated Inversion Recovery (FLAIR)

For cord disease, the primary sequence goal is contrast, with resolution assuming much less importance. Fast fluid-attenuated inversion recovery (FLAIR) is an SE sequence with a long inversion time (TI) that suppresses the signal from CSF (Fig 5). This pulse, coupled with a long TR/TE, gives the benefits of a T2-weighted image without the

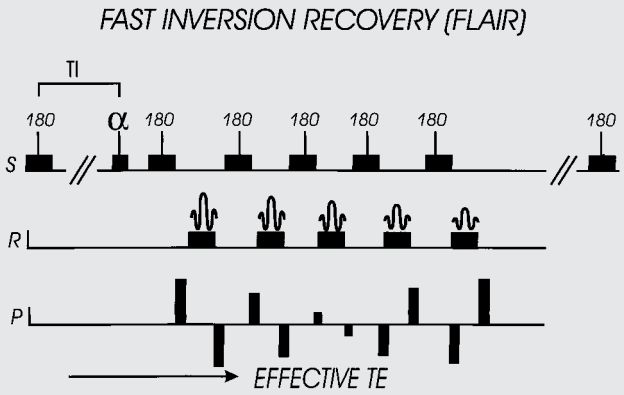

FIG 5. Fast FLAIR sequence structure. Typical FSE sequence structure of multiple 180° pulses is modified by addition of a 180° inversion pulse, followed by a delay time until the alpha pulse (inversion time or TI). CSF is suppressed by appropriate selection of inversion time, which for FLAIR is approximately 2000 ms. Effective TE is determined by low-amplitude phase-encoding steps (central k-space). S = slice-select direction, R = "read" or frequency-encode direction, P = phase-encode direction.

interfering high signal from CSF. Despite the long acquisition time (>12 min) of the early sequence iterations that did not have the advantage of the FSE technique, the clinical usefulness in brain imaging was obvious. Evaluation of a wide variety of intracranial diseases are performed with FLAIR quite successfully (18, 23–25). The use of FLAIR for evaluation of the spinal cord is a natural progression of this technique, given the difficulties encountered with CSF pulsation artifacts on T2-weighted FSE images. The possibility of a T2 sequence with low CSF signal was enticing because it might improve detection of subtle cord surface lesions. The FSE implementation of FLAIR has markedly reduced imaging times, while maintaining this unique sequence contrast.

The application of FLAIR for spinal cord imaging has not, however, been as straightforward as for brain imaging, and there are widely divergent opinions of its usefulness. Advocates recommend using FLAIR as the primary sequence for intramedullary disease, whereas opponents argue that it's useless or misleading because of lesions missed (10, 26–31). The latter is my admittedly biased opinion. The breakdown of the relevant articles addressing FLAIR is presented in Table 1, focusing on patients with multiple sclerosis (MS) as the archetypal cord lesion.

The literature is difficult to assess because of the widely divergent techniques discussed. Multiple parameters are varied in the different studies, including field strength, coil, slice thickness, field of view, echo train and spacing, matrix, and selective vs nonselective pulses. Nevertheless, personal experience has tipped our interpretation of the literature strongly away from using FLAIR in the evaluation of spinal cord disease (Fig 6). We continue to use FLAIR as part of routine brain evaluation.

Why is FLAIR so variable, and at times so insensitive to intramedullary disease? This failure would have direct clinical impact, as isolated spinal cord involvement occurs in 15–20% of MS patients (32), and finding cord lesions is more specific for the diagnosis than cerebral white matter lesions (33). Various causes have been postulated. Stevenson et al (31) theorized that there might be an intrinsic difference in cerebral hemispheric lesions and cord lesions giving rise to a shorter T2 for cord. The concept of a fundamental pathologic difference in brain and cord MS lesions is also shared by Filippi et al (30), although they recognize the variable imaging parameters (TR/TE/TI) also as another source of difficulty.

The presence of flow artifacts may also degrade FLAIR images acquired with section-selective inversion pulses (25). The pulsatile nature of CSF creates spins that are not affected by the inversion pulse, and therefore do not enter the slice during the inversion interval, producing high-signal intensity on the subsequent FSE image. This high signal could potentially mask adjacent cord disease. This effect can be considered analogous to the entry-slice phenomenon seen on GE imaging. This problem is not present with a nonselective inversion pulse as used by White and Thomas (26, 27). The downside of the nonselective pulse is that each slice will have a slightly different inversion time, although this is not reported as a major limitation for sagittal spinal imaging with few slices. Nonetheless, the poor lesion detection of fast FLAIR with a selective inversion pulse occurs even in the face of very good CSF signal suppression, and so the selective pulse most likely is a minor component of lesion conspicuity degradation.

Perhaps more to the point is simply the heavy T2 weighting of the fast FLAIR sequence that diminishes cord lesion contrast, as pointed out by Hittmair (10). Care must be exercised to avoid

TABLE 1: FLAIR and MS in the cord

Author	Summary	No. of MS Patients	Sequence	TR/TE/TI (approximate)
White et al, 1992	FLAIR good	3	Conventional FLAIR	6000/20–90/2200
Thomas et al, 1993	FLAIR good	16	Conventional FLAIR	6000/120/2100
Hajnal et al, 1995	FLAIR good	2	Fast FLAIR	6000/60/2200
Keiper et al, 1997	FLAIR bad	15	Fast FLAIR	4000–11000/100–150/1500–2600
Hittmair et al, 1996	FLAIR bad	20	Fast FLAIR	6000/120/2000
Filippi et al, 1996	FLAIR bad	13	Fast FLAIR	9000/105/2200
Stevenson et al, 1997	FLAIR bad	10	Fast FLAIR	11000/144/2150

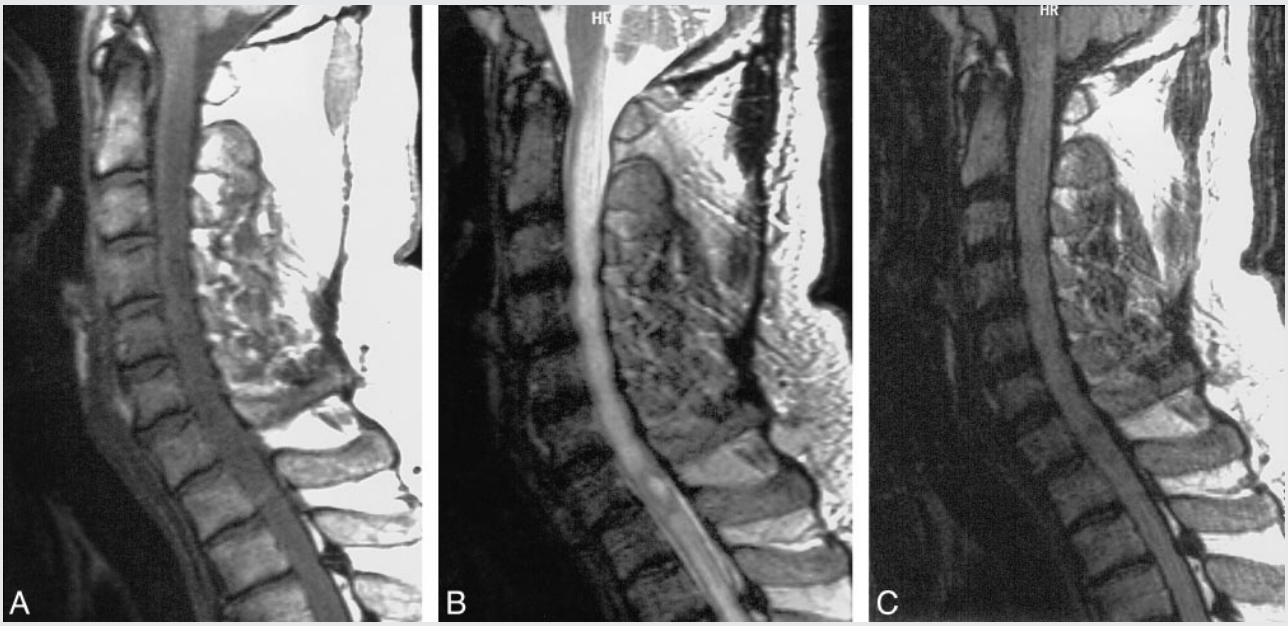

FIG 6. False-negative fast FLAIR for demyelinating disease.
A, Sagittal T1-weighted image (500/12/2) demonstrates a markedly enlarged cord with slighted decreased signal centrally.
B, Sagittal T2-weighted FSE (4620/112/ 3) shows diffuse increased signal throughout cervical cord.
C, Sagittal FSE FLAIR (6000/105/ 2) shows low signal at C7-T1 level, but no abnormal increased signal as on the FSE.

equating pretty images with bright CSF signal and a sharp cord/CSF interface with good intramedullary lesion detection. FSE and fast FLAIR sequences may have flaws in this regard. Both yield pleasing image quality with low apparent artifacts, but all too often fail to reveal a lesion because of very heavy T2 weighting. Most cord disease will have both prolonged T1 and T2, and a sequence that is heavily T2-weighted will diminish lesion contrast. This problem is further compounded by the long-echo trains employed, which have a large amount of T2 decay that blur images. The FSE sequence that can give a good CSF myelographic image for degenerative disk disease is not the sequence to use for intramedullary disease.

Short-Inversion-Time Inversion Recovery (STIR)

Short-inversion-time inversion recovery (STIR) has shown a high sensitivity for musculoskeletal disease because of the synergistic effects of prolonged T1 and T2 in abnormal tissues, coupled with the improved C/N and fat suppression (Fig 7) (34–36). This technique has been favorably compared to T1- and T2-weighted FSE, CSE, and fat saturated FSE in the detection of vertebral metastatic disease (37–39).

The use of STIR, and especially fast STIR, for intramedullary disease is perhaps less well known. In the analysis by Hittmair et al (10), the fast STIR sequence was best for revealing MS lesions, and showed lesions that were missed with other, more routine techniques, such as FSE. Their technique included asymmetric sampling with one echo collected before and six echos collected after the TE effective (echo train of 8), six averages, and a cephalocaudal phase-encoding direction. The cephalocaudal phase-encoding direction is typical for FSE sagittal spine sequences. The fast STIR will require a slightly shorter TI and more signal averages than the conventional STIR sequence because of the contribution of stimulated echos (40). The overall image quality tends to be rather noisy, but the usefulness is provided by the high C/N. This technique appears to be very useful for cervical cord disease, but is more prone to motion artifact and falls short in the evaluation of thoracic cord disease. We have found that satisfactory sagittal fast STIR images can be obtained with the following parameters: 1200/14/175, 192 x 256 matrix, 3-mm slice thickness, ETL = 3, coronal saturation pulse, time = 3:56 (Figs 8 and 9). A summary of the articles related to STIR and the cord are presented in Table 2.

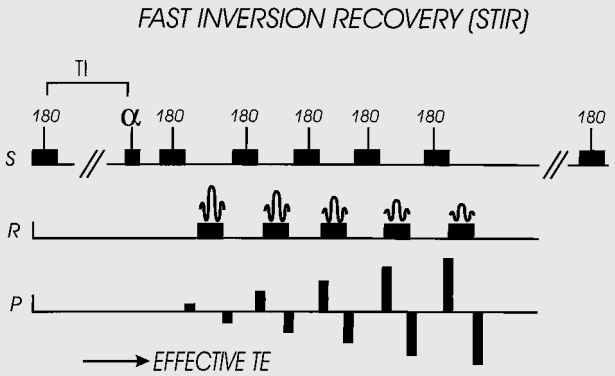

FIG 7. Fast STIR sequence structure. This is analogous to FLAIR sequence, except that TI time is shorter to null fat signal, and low-amplitude phase-encode steps are acquired earlier. S = slice-select direction, R = ''read'' or frequency- encode direction, P = phase-encode direction.

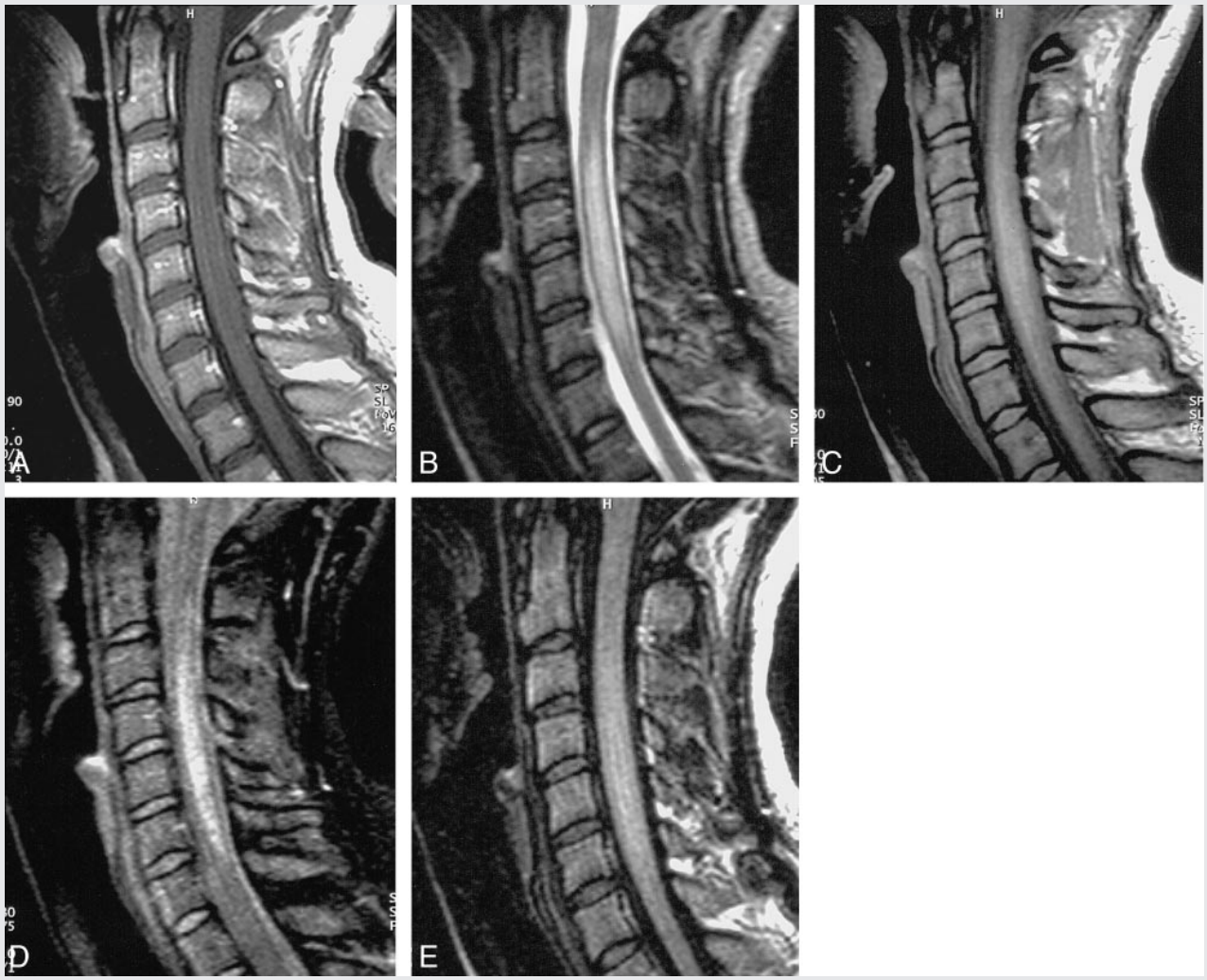

FIG 8. T2W vs. FLAIR vs. STIR in demyelinating disease.
A, Fusiform enlargement of cord without enhancement is shown on sagittal T1-weighted sequence (500/12/2).
B, Abnormal high signal within cord is shown on sagittal FSE T2-weighted sequence (4620/112/ 3).
C and *D,* FSE spin-density weighted (2000/10/2), and FSE STIR (1200/14/4), respectively.
E, Abnormal cord signal is not revealed by fast FLAIR sequence (6000/105/ 2). Lesion is most conspicuous on FSE T2-weighted and fast STIR sequences.

Diffusion-Weighted Imaging

Diffusion-weighted imaging (DWI) has been used extensively for the evaluation of brain disease, specifically for the detection of acute infarcts (41–44). Acute infarcts have cytotoxic edema causing cellular swelling and diminished interstitial space. This decreased space restricts diffusion. DWI has also been applied to characterize other diseases such as epilepsy, brain tumors, and demyelinating disease (13, 45, 46).

Applying DWI for spine imaging has been limited relative to brain imaging, mainly because of the technical constraints imposed by motion and bone artifact. Most DWI of the cord is performed in vitro, and relates to the evaluation of posttraumatic change (47–48). The use of DWI for in vivo human cord imaging is in its infancy (Fig 10). A variety of techniques have been evaluated for in vivo cord imaging including steady-state gradient, SE, echo-planar imaging (EPI), and GE EPI. Gradient-echo EPI appears the least useful because of its tremendous susceptibility to artifacts from the bony canal. Spin-echo EPI has shown cord abnormalities in a small number of traumatic and myelopathic cases (49, 50). Apparent diffusion coefficient maps have also been generated from a gated SE technique (51).

Extramedullary/Bony Abnormalities

For evaluation of degenerative disk disease, resolution now assumes a more dominant role relative to contrast. As sequences have evolved, the matrices have increased, and slice thickness has diminished. Two-dimensional image evaluation of the neural foramina for osteophyte or lateral disk herniations is best accomplished by axial imaging. High-signal-intensity CSF-type images are generally preferred because of the problem of visualizing low-signal-intensity ligaments or osteophytes against the dark CSF images on T1-weighted

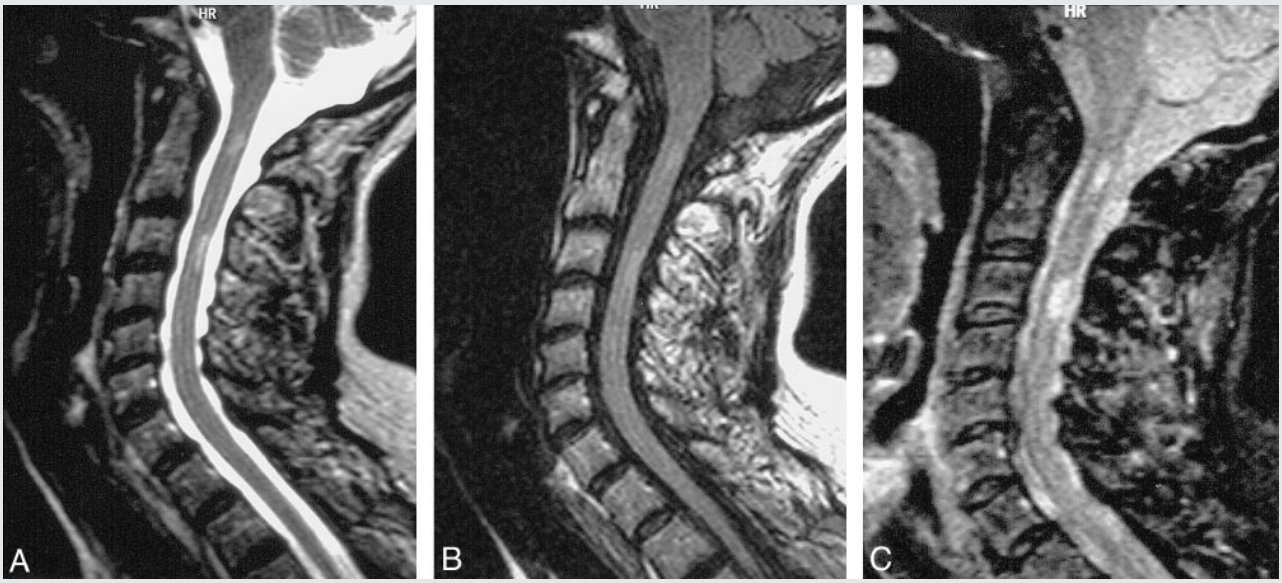

FIG 9. Chronic demyelinating disease.
A, Sagittal T2-weighted FSE (4620/112/ 3) shows faint focal increased signal in cervical cord at C1 and C3 levels.
B, Sagittal FSE FLAIR (6000/105/2) also shows very indistinct abnormal signal at those two levels.
C, High lesion-to-cord contrast is achieved with fast STIR sequence (1200/14/4).

TABLE 2: STIR and cord disease

Author	Summary	No. of Patients	Sequences	TR/TE/TI (approximate)
Thorpe et al, 1994	STIR good	17	Fast STIR	1500/51/175
Mascalchi et al, 1993	STIR good	21	Conventional STIR	1000–1400/30–120/100
Hittmair et al, 1996	STIR good	20	Fast STIR	2165/50/110

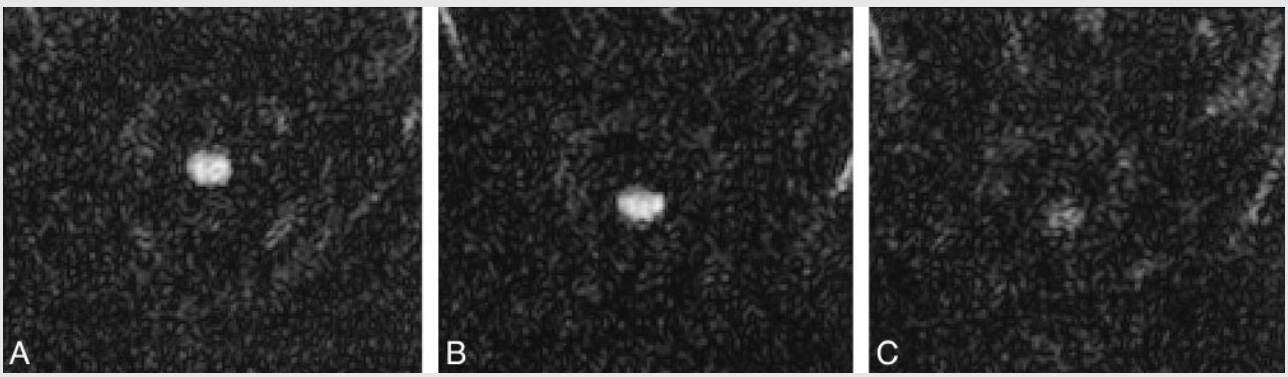

FIG 10. Echo-planar diffusion imaging of the normal cervical cord. Three orthogonal directions of diffusion gradients are applied: anteroposterior (*A*); transverse (*B*); and through-plane (*C*). Notice the least signal from the cord with through-plane diffusion encoding (*parallel to white matter tracts*) reflecting direction of relatively fastest water diffusion.

images. The now-classic articles by Enzmann and Rubin (52, 53) defined the templates for partial flip angle GE technique for the detection of cervical disk disease. Others subsequently confirmed this technique (54–56). The parameters manipulated to change S/N and contrast included flip angle, TR, and TE. For cervical disk disease, Enzmann et al recommended a small flip angle (3–8°) for the best contrast for disk, cord, and CSF. TR should be kept as short as possible because this reduces imaging time, and these sequences are sensitive to motion artifacts. TE should be kept short as well, because this minimizes magnetic susceptibility artifacts that may exaggerate the severity of foraminal stenosis. Table 3 summarizes bright CSF GE sequences for the cervical spine.

The major problem of 2D MR imaging techniques in diagnosing cervical disease is its inability to reveal foraminal disease accurately because of long echo times, relatively thick image slices (3–5 mm), and views of exiting nerve roots limited to the axial plane (57). Although overall examination times have decreased with GE imaging, the length of examinations continues to be problematic.

TABLE 3: Bright CSF GE imaging and the cervical spine

Authors	Sequence	TR	TE	Flip Angle	Slice Thickness/ Acquisitions	MT Contrast
Enzmann 1988	2D GRASS	22–60	12.5–25.0	3–8°	5mm/8 acq	no
Hedberg et al, 1988	2D GRASS	75	12.3	10°	5mm/4 acq	no
Kulkarni et al, 1988	2D GE	750	9.0	30°	5mm/4 acq	no
Tsuruda et al, 1989	3D GE	35	15.0	5°	1.5–2mm/2 acq	no
Katz et al, 1989	2D GE	300	14.0	10°	5mm/4 acq	no
Youssem et al, 1991	3D GE	50	15.0	5°	1.5mm	no
Yoshoika et al, 1994	2D GE (0.3 T)	750	23.0	25°	5mm/2 acq	yes
Finelli et al, 1994	2D GE	1367	18.0	45°	3mm	yes
Lycklama et al, 1996	2D GE	616	22.0	20°	3mm/4	yes
Melhem et al, 1996	3D GE	39	6.0	5°	1.5mm/1	yes

One solution to these problems is found in GE volume imaging, a 3D technique that allows short TEs with thin contiguous slices and the reformating of data in any desired viewing plane (58). In 3D imaging, a volume of interest is defined by the initial radiofrequency (RF) excitation pulse instead of by a thin slice such as in 2D imaging. This volume of tissue can then be divided into thin contiguous slices by the addition of phase encoding along the slice-select direction. When phase encoding is used in two different directions, the imaging time is proportionally increased by the number of slices selected (imaging time = TR × number of excitations × number of in-plane phase-encoding steps × number of partitions), as compared with 2D imaging times. The theoretical advantages of 3D over 2D imaging include increased S/N, and thin contiguous slices with a more accurate slice thickness that can be obtained without the problem of crosstalk (59–61). Three-dimensional GE imaging has two major drawbacks for routine cervical spine imaging. The first is the necessity of using a low flip angle (approximately 5°) to produce the desired high-signal CSF. The low flip angle gives low S/N, and the all-too-familiar grainy image. The second problem is the sensitivity of the sequence to motion artifacts. Our standing routine for cervical degenerative disease includes a 3D GE axial sequence, with the backup of a 2D GE because patient motion degrades image quality. One technique that shows great promise in reducing these problems is magnetization transfer (MT).

Magnetization Transfer

Magnetic transfer (MT) imaging is based on the differences between ''bound'' water protons associated with macromolecules (proteins and cell membranes) and free or ''bulk'' water protons. The application of an off-resonance pulse will saturate the bound water protons, leading to the transfer of some saturation from the bound water to the bulk water protons via dipole-dipole interactions and chemical exchanges (62–64). In practical terms, this means that the addition of an easily implemented MT pulse to a sequence can generate a new contrast mechanism. This contrast technique can be looked at quantitatively, as has been done for MS lesions in the brain. Another approach is to add the MT pulse to a routinely used sequence as an image C/N modifier. The most widespread applications of this intrinsic contrast modification are TOF MR angiographic techniques, and SE contrast-enhanced brain imaging. In these sequences, MT acts as a background suppression technique to allow improved MIP MR angiographic projections and enhanced lesion detection, respectively (65–69).

In spine imaging, the use of MT may give several benefits as described by Finelli (70). The addition of the MT pulse increases the sensitivity of the GE images to intramedullary disease, such as MS plaques. The intervertebral disk shows moderate MT suppression, so the addition of the MT pulse improves contrast between the disk and the adjacent CSF. The improved contrast of the MT GE images could be traded off against higher resolution images, which is always of concern in cervical spine imaging (Fig 11). The downside of MT is diminished definition of the disk space on the axial images, which makes defining the anatomic level slightly more difficult. Finally, Melhem et al described an important additional advantage of the high-contrast MT GE sequences, namely that the high signal of CSF could be maintained with a much shorter TE (71). This short TE would minimize the magnetic susceptibility effect that causes an exaggeration of foraminal stenosis (72).

Steady-State Sequences

True fast imaging with steady-state precession (FISP), a sequence that has been around since the early days of GE imaging, has more recently made a resurgence for neurologic imaging (Fig 12) (73, 74). Steady-state sequences with balanced gradients (i.e., True FISP and CISS) have the advantage of providing high-signal-intensity CSF with higher flip angles. The high flip angle gives better S/N. True FISP is considered ''true'' because the net effect of the imaging gradients on transverse phase evolution is zero, whereas it is constant but nonzero for the more generic FISP. The zero-net effect of the gradients allows spins that are stationary, as well as those moving with constant velocity to

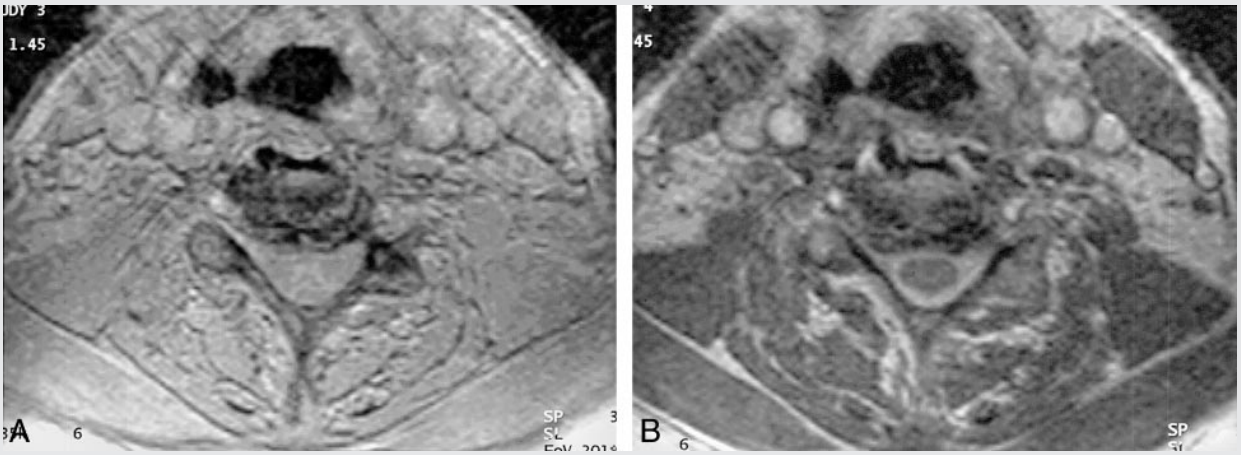

FIG 11. MT contrast. Axial gradient echo slice without (*A*) and with (*B*) application of off-resonance MT pulse. Application of MT dramatically improves cord/CSF contrast.

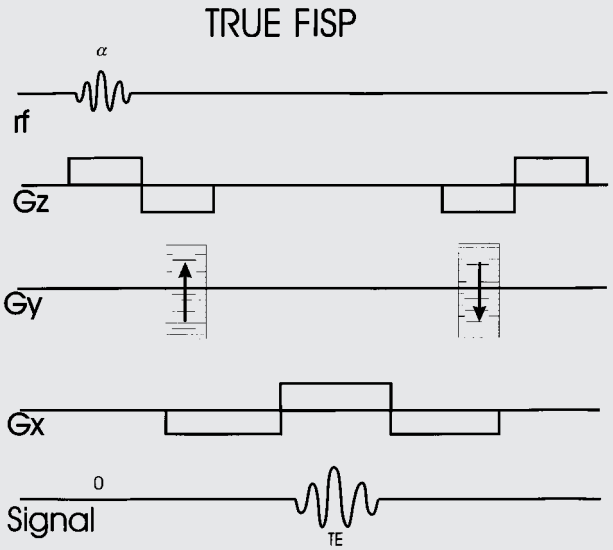

FIG 12. True FISP sequence structure with balanced gradients. Net effect of gradients allows spins that are stationary as well as those moving with constant velocity to reach a steady state. Gz = slice select gradient, Gy = phase encode gradient, and Gx = frequency encode gradient.

reach a steady state. Only the stationary spins achieve a steady state in the more generic FISP.

The problem with these steady-state balanced-gradient sequences, and why they did not make a great impact for imaging at high-field strengths, was the presence of a dark banding pattern across the images (Fig 13). This banding occurs because steady-state sequences are also dependent upon the resonant offset angle (β), the phase angle through which the spins process between sequential RF pulses. This variation in β occurs with field inhomogeneities and imperfections in gradient refocusing. Various techniques are available to address this problem, such as phase alternating the successive RF pulses, or obtaining separate acquisitions with 0° and 180° phase offset, and combining the images. This sequence provides a rapid method of achieving high-signal CSF with good S/N. The downside of this sequence is its relatively poor soft-tissue contrast. Applications in the brain have focused on a 3D technique and visualization of the inner ear (75). For the spine, CISS allows for good visualization of the intradural cervical roots, and might be useful for a more general evaluation of cervical degenerative disease when combined with a technique better suited for evaluation of the foramina, such as axial FSE or 3D GE (Fig 14) (76). This technique has also been successfully applied to imaging posttraumatic brachial plexus injuries, with the axial native images allowing definition of the avulsed roots, and the 3D MIP projections displaying the meningoceles (77). Steady-state sequences have also had been used for 3D MR myelography (78, 79).

True FISP also appears useful as a localization method for MR-guided interventions at low-field strength (0.2 T) (80). The problem of resonant offset and the banding pattern is not of such concern at low-field strength simply because low-field strength corresponds to lower resonant frequency, and consequently less resonant offset. True FISP in this particular setting gives single-slice images with good contrast in less than 2 s (TR $<$ 12 ms).

Diffusion

Baur et al (81) used a steady-state free precession sequence (SSFP) (a.k.a. contrast-enhanced Fourier acquired steady-state technique [CE-FAST], and reversed fast imaging with steady-state precession, collection of the refocused echo [PSIF]) with added diffusion-sensitive gradients to distinguish malignant from benign vertebral compression fractures in 30 patients (Fig 15). This is a tantalizing concept for a notoriously difficult imaging differential diagnosis. The underlying theory is that, with a benign fracture, the marrow edema will allow relatively increased diffusion, making the vertebral bodies dark on the SSFP diffusion sequence relative to normal marrow. Conversely, the cellular

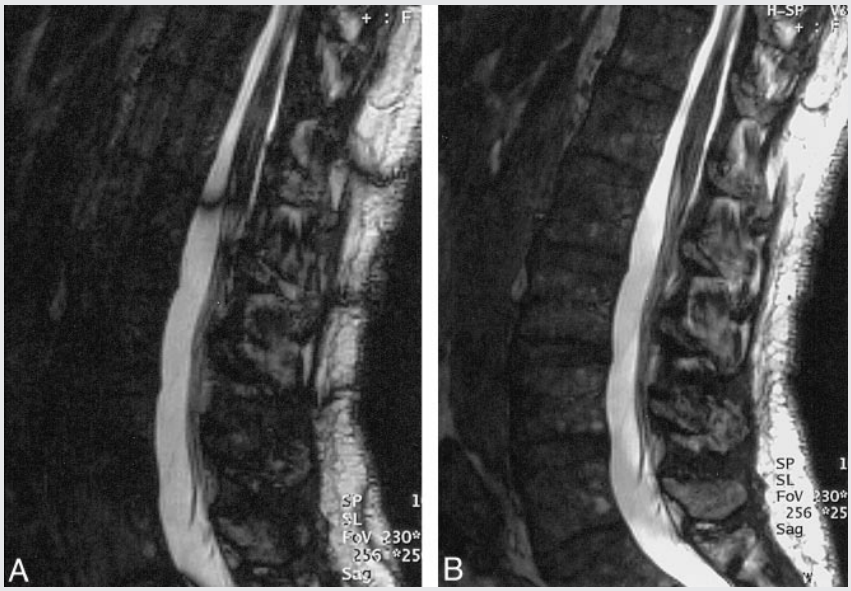

FIG 13. True FISP (17/8/2, 70° flip angle).
A, Sagittal 2-mm slice from one of the two sequences acquired with different RF phase (combined to produce final image) demonstrates areas of banding or signal loss related to nonuniform resonant offset.
B, Combined final sequence shows more uniform high-signal CSF with relative suppression of soft-tissue signal.

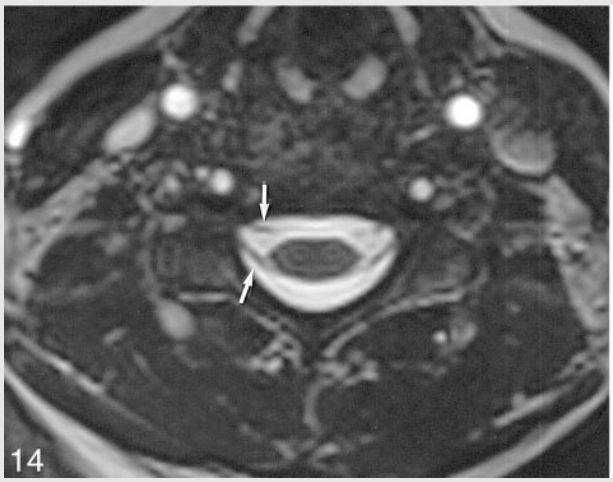

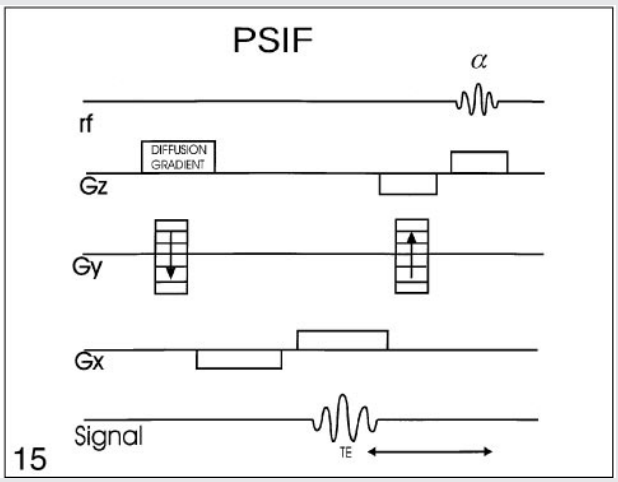

FIG 14. 3D CISS (12/6/3, 70° flip angle). Axial 2-mm section through cervical spine shows sharp interface between cord/intradural dorsal and ventral roots (*arrows*) and the CSF. There is slight truncation artifact surrounding the cord, manifest as curvilinear low signal.

FIG 15. PSIF diffusion-sequence structure (aka, FISP backwards).Diffusion weighting is applied as a single gradient along slice-select direction. Acquired signal is an RF echo. Echo occurs prior to alpha pulse because it is generated by the refoccussing of magnetization that has resided in transverse plane over at least one previous complete TR cycle. Gz = slice-select gradient, Gy = phase- encode gradient, Gx = frequency-encode gradient.

elements of a malignant fracture will restrict diffusion, allowing for increased signal on the native images. This technique has problems, and additional studies need to be done confirming this potentially very important finding. Le Bihan (82) notes in the accompanying editorial on the Baur article that the SSFP sequence cannot be quantified because the confounding effects of T1, T2, and diffusion are not easy to separate, as is the case with an SE diffusion sequence. Further, the SSFP sequence Baur used had fairly low diffusion sensitization (the b factor), on the order of 165 s/mm^2. Typical brain diffusion studies routinely have b factors on the order of 1000 s/mm^2. Although a higher b factor was tested in a small group of patients in the Baur study, it did not yield more information, and suffered from diminished S/N. Our anecdotal experience with this technique has been somewhat variable (Figs 16 and 17). More experience is needed to determine if this technique can effectively differentiate malignant from benign findings for compression fractures.

Conclusion

After all is said and done, where are we headed with spinal MR imaging? In a perfect world, only a few very robust sequences would be required for the complete evaluation of the spinal axis, with high S/N and lesion contrast, and no artifacts. Realistically, the future holds an even wider array of sequences and techniques that will be most useful for specific areas of disease, and will require a greater degree of tailoring. Perhaps as critical as

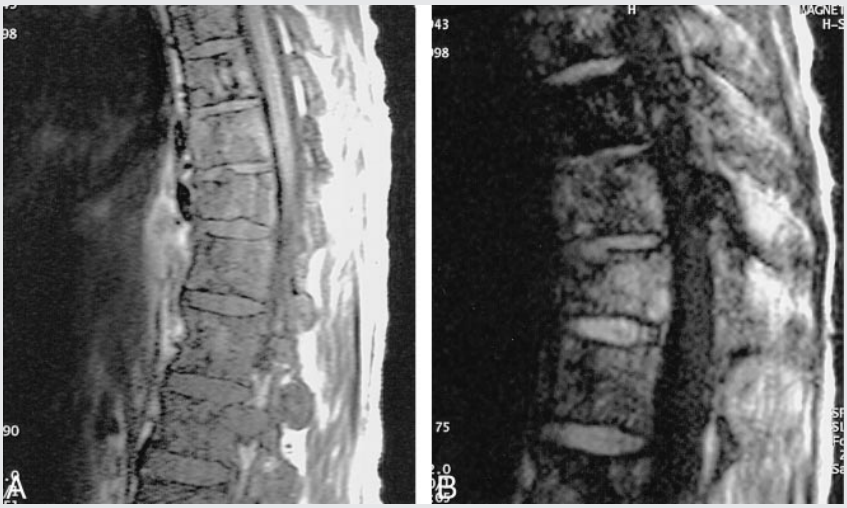

FIG 16. Diffusion true positive in patient with myeloma (PSIF 22/2/10, 75° flip angle).

A, Sagittal T1-weighted image shows diffuse abnormal marrow signal with mild compression fracture.

B, Sagittal PSIF sequence with diffusion gradient shows high signal from compression fracture comfirming malignant origin.

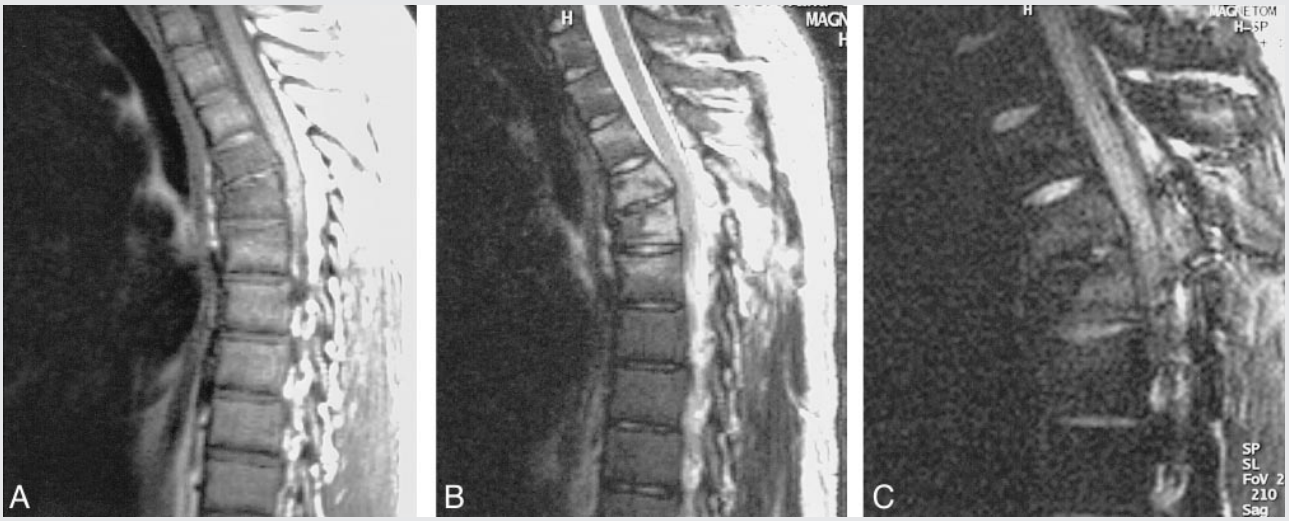

FIG 17. Diffusion false positive in trauma (PSIF 22/2/10, 75° flip angle) found in a 17-year-old who sustained a flexion injury at C3–4 after going over handlebars of waterski.

A and *B,* Sagittal T1-weighted (*A*) and T2-weighted (*B*) images show anterior wedge deformities of C3 and C4 bodies.

C, Diffusion sequence shows slight increased signal from bodies, falsely suggesting a cellular infiltrate.

the native sequences are the sources of artifact and error related to data manipulations such as interpolation, data sharing, and synthesis. Diligence and tenacity will be required to tease out the specifics of an imaging sequence that will allow better image interpretation in light of its specific structure, and will maintain the premier role that MR has achieved in the evaluation of spinal diseases.

Acknowledgments

I would like to thank Mike Modic, Daniel Finelli, and Jean Tkach for their help in the preparation of this manuscript.

References

1. Aagaard BD, Maravilla KR, Kliot M. **MR neurography. MR imaging of peripheral nerves.** *Magn Reson Imaging Clin N Am* 1998;6:179–194
2. Maravilla KR, Bowen BC. **Imaging of the peripheral nervous system: evaluation of peripheral neuropathy and plexopathy.** *AJNR Am J Neuroradiol* 1998;19:1011–1023
3. Georgy BA, Hesselink JR. **MR imaging of the spine: recent advances in pulse sequences and special techniques.** *AJR Am J Roentgenol* 1994;162:923–934
4. Jones KM, Mulkern RV, Schwartz RB, Oshio K, Barnes PD, Jolesz FA. **Fast spin-echo MR imaging of the brain and spine: current concepts.** *AJR Am J Roentgenol* 1992;158:1313–1320
5. Sze G, Kawamura Y, Negishi C, Constable RT, Merriam M, Oshio K, Jolesz F. **Fast spin-echo MR imaging of the cervical spine: influence of echo train length and echo spacing on image contrast and quality.** *AJNR Am J Neuroradiol* 1993;14:1203–1213
6. Yuan C, Schmiedl UP, Weinberger E, Krueck WR, Rand SD. **Three-dimensional fast spin-echo imaging: pulse sequence and in vivo image evaluation.** *J Magn Reson Imaging* 1993;3:894–899
7. Oshio K, Jolesz FA, Melki PS, Mulkern RV. **T2-weighted thin-section imaging with the multislab three-dimensional RARE technique.** *J Magn Reson Imaging* 1991;1:695–700
8. Murakami JW, Weinberger E, Tsuruda JS, Mitchell JD, Yuan C. **Multislab three-dimensional T2-weighted fast spin-echo imaging of the hippocampus: sequence optimization.** *J Magn Reson Imaging* 1995;5:309–315
9. Constable RT, Gore JC. **The loss of small objects in variable TE imaging: implications for FSE, RARE, and EPI.** *Magn Reson Med* 1992;28:9–24
10. Hittmair K, Mallek R, Prayer D, Schindler EG, Kollegger H. **Spinal cord lesions in patients with multiple sclerosis: Comparison of MR pulse sequences.** *AJNR Am J Neuroradiol* 1996;17:1555–1565

11. Le Bihan D, Breton E, Lallemand D, Grenier P, Cabanis E, Laval-Jeantet M. **MR imaging of intravoxel incoherent motions: application to diffusion and perfusion in neurologic disorders.** *Radiology* 1986;161:401–407
12. Le Bihan D. **Intravoxel incoherent motion imaging using steady-state free precession.** *Magn Reson Med* 1988;7:346–351
13. Le Bihan D, Turner R, Douek P, Patronas N. **Diffusion MR imaging: clinical applications.** *AJR Am J Roentgenol* 1992;159: 591–599
14. Rudisch A, Kremser C, Peer S, Kathrein A, Judmaier W, Daniaux H. **Metallic artifacts in magnetic resonance imaging of patients with spinal fusion. A comparison of implant materials and imaging sequences.** *Spine* 1998;23:692–699
15. Mathews VP, Greenspan SL, Caldemeyer KS, Patel MR. **FLAIR and HASTE imaging in neurologic diseases.** *Magn Reson Imaging Clin N Am* 1998;6:53–65
16. Naganawa S, Itoh T, Fukatsu H, Ishigaki T, Nakashima T, Kassai Y, Miyazaki M, Takai H. **Three-dimensional fast spin-echo MR of the inner ear: ultra-long echo train length and half-Fourier technique.** *AJNR Am J Neuroradiol* 1998;19:739–741
17. Du YP, Parker DL, Davis WL, Cao G. **Reduction of partial-volume artifacts with zero-filled interpolation in three-dimensional MR angiography.** *J Magn Reson Imaging* 1994;4:733–741
18. Filippi M, Yousry T, Baratti C, Horsfield MA, Mammi S, Becker C, Voltz R, Spuler S, Campi A, Reiser MF, Comi G. **Quantitative assessment of MRI lesion load in multiple sclerosis. A comparison of conventional spin-echo with fast fluid-attenuated inversion recovery.** *Brain* 1996;119:1349–1355
19. Thorpe JW, Halpin SF, MacManus DG, Barker GJ, Kendall BE, Miller DH. **A comparison between fast and conventional spin-echo in the detection of multiple sclerosis lesions.** *Neuroradiology* 1994;36:388–392
20. Sze G, Merriam M, Oshio K, Jolesz FA. **Fast spin-echo imaging in the evaluation of intradural disease of the spine.** *AJNR Am J Neuroradiol* 1992;13:1383–1392
21. Chappell PM, Glover GH, Enzmann DR. **Contrast on T2-weighted images of the lumbar spine using fast spin-echo and gated conventional spin-echo sequences.** *Neuroradiology* 1995;37: 183–186
22. Ross JS, Ruggieri P, Tkach J, Obuchowski N, Dillinger J, Masaryk TJ, Modic MT. **Lumbar degenerative disk disease: Prospective comparison of conventional T2-weighted spin-echo imaging and T2-weighted rapid acquisition relaxation-enhanced imaging.** *AJNR Am J Neuroradiol* 1993;14:1215–1223
23. De Coene B, Hajnal JV, Gatehouse P, Longmore DB, White SJ, Oatridge A, Pennock JM, Young IR, Bydder GM. **MR of the brain using fluid-attenuated inversion recovery (FLAIR) pulse sequences.** *AJNR Am J Neuroradiol* 1992;13:1555–1564
24. Hajnal JV, Bryant DJ, Kasuboski L, Pattany PM, De Coene B, Lewis PD, Pennock JM, Oatridge A, Young IR, Bydder GM. **Use of fluid attenuated inversion recovery (FLAIR) pulse sequences in MRI of the brain.** *J Comput Assist Tomogr* 1992;16:841–844
25. Hashemi RH, Bradley WGJ, Chen DY, Jordan JE, Queralt JA, Cheng AE, Henrie JN. **Suspected multiple sclerosis: MR imaging with a thin-section fast FLAIR pulse sequence.** *Radiology* 1995;196:505–510
26. White SJ, Hajnal JV, Young IR, Bydder GM. **Use of fluid-attenuated inversion-recovery pulse sequences for imaging the spinal cord.** *Magn Reson Med* 1992;28:153–162
27. Thomas DJ, Pennock JM, Hajnal JV, Young IR, Bydder GM, Steiner RE. **Magnetic resonance imaging of spinal cord in multiple sclerosis by fluid-attenuated inversion recovery.** *Lancet* 1993;341:593–594
28. Hajnal JV, Kasuboski L, De SN, Bydder GM. **Magnetic resonance imaging: Spinal cord imaging with the turbo-fluid attenuated inversion recovery (FLAIR) pulse sequence.** *Clin Radiol* 1995;50:1–5
29. Keiper MD, Grossman RI, Brunson JC, Schnall MD. **The low sensitivity of fluid-attenuated inversion-recovery MR in the detection of multiple sclerosis of the spinal cord.** *AJNR Am J Neuroradiol* 1997;18:1035–1039
30. Filippi M, Yousry TA, Alkadhi H, Stehling M, Horsfield MA, Voltz R. **Spinal cord MRI in multiple sclerosis with multicoil arrays: A comparison between fast spin echo and fast FLAIR.** *J Neurol Neurosurg Psychiatry* 1996;61:632–635
31. Stevenson VL, Gawne CM, Barker GJ, Thompson AJ, Miller DH. **Imaging of the spinal cord and brain in multiple sclerosis: A comparative study between fast flair and fast spin echo.** *J Neurol* 1997;244:119–124
32. Edwards MK, Farlow MR, Stevens JC. **Cranial MR in spinal cord MS: diagnosing patients with isolated spinal cord symptoms.** *AJNR Am J Neuroradiol* 1986;7:1003–1005
33. Thorpe JW, Kidd D, Moseley IF, Thompson AJ, MacManus DG, Compston DA, McDonald WI, Miller DH. **Spinal MRI in patients with suspected multiple sclerosis and negative brain MRI.** *Brain* 1996;119:709–714
34. Dwyer AJ, Frank JA, Sank VJ, Reinig JW, Hickey AM, Doppman JL. **Short-Ti inversion-recovery pulse sequence: analysis and initial experience in cancer imaging.** *Radiology* 1988;168:827–836
35. Mehta RC, Marks MP, Hinks RS, Glover GH, Enzmann DR. **MR evaluation of vertebral metastases: T1-weighted, short-inversion-time inversion recovery, fast spin-echo, and inversion-recovery fast spin-echo sequences.** *AJNR Am J Neuroradiol* 1995; 16:281–288
36. Weinberger E, Shaw DW, White KS, Winters WD, Stark JE, Nazar-Stewart V, Hinks RS. **Nontraumatic pediatric musculoskeletal MR imaging: comparison of conventional and fast-spin-echo short inversion time inversion-recovery technique.** *Radiology* 1995;194:721–726
37. Hilfiker P, Zanetti M, Debatin JF, McKinnon G, Hodler J. **Fast spin-echo inversion-recovery imaging versus fast T2-weighted spin-echo imaging in bone marrow abnormalities.** *Invest Radiol* 1995;30:110–114
38. Baker LL, Goodman SB, Perkash I, Lane B, Enzmann DR. **Benign versus pathologic compression fractures of vertebral bodies: assessment with conventional spin-echo, chemical-shift, and STIR MR imaging.** *Radiology* 1990;174:495–502
39. Jones KM, Schwartz RB, Mantello MT, Ahn SS, Khorasani R, Mukherji S, Oshio K, Mulkern RV. **Fast spin-echo MR in the detection of vertebral metastases: comparison of three sequences.** *AJNR Am J Neuroradiol* 1994;15:401–407
40. Hittmair K, Trattnig S, Herold CJ, Breitenseher M, Kramer J. **Comparison between conventional and fast spin-echo stir sequences.** *Acta Radiol* 1996;37:943–949
41. Fisher M, Prichard JW, Warach S. **New magnetic resonance techniques for acute ischemic stroke.** *JAMA* 1995;274:908–911
42. Warach S, Dashe JF, Edelman RR. **Clinical outcome in ischemic stroke predicted by early diffusion-weighted and perfusion magnetic resonance imaging: a preliminary analysis.** *J Cereb Blood Flow Metab* 1996;16:53–59
43. Moseley ME, Butts K, Yenari MA, Marks M, de Crespigny A. **Clinical aspects of DWI.** *NMR Biomed* 1995;8:387–396
44. Sorensen AG, Buonanno FS, Gonzalez RG, Schwamm LH, Lev MH, Huang-Hellinger FR, Reese TG, Weisskoff RM, Davis TL, Suwanwela N, Can U, Moreira JA, Copen WA, Look RB, Finklestein SP, Rosen BR, Koroshetz WJ. **Hyperacute stroke: evaluation with combined multisection diffusion-weighted and hemodynamically weighted echo-planar MR imaging.** *Radiology* 1996;199:391–401
45. Tofts PS. **Novel MR image contrast mechanisms in epilepsy.** *Magn Reson Imaging* 1995;13:1099–1106
46. Horsfield MA, Lai M, Webb SL, Barker GJ, Tofts PS, Turner R, Rudge P, Miller DH. **Apparent diffusion coefficients in benign and secondary progressive multiple sclerosis by nuclear magnetic resonance.** *Magn Reson Med* 1996;36:393–400
47. Ford JC, Hackney DB, Alsop DC, Jara H, Joseph PM, Hand CM, Black P. **MRI characterization of diffusion coefficients in a rat spinal cord injury model.** *Magn Reson Med* 1994;31:488–494
48. Pattany PM, Puckett WR, Klose KJ, Quencer RM, Bunge RP, Kasuboski L, Weaver RG. **High-resolution diffusion-weighted MR of fresh and fixed cat spinal cords: evaluation of diffusion coefficients and anisotropy.** *AJNR Am J Neuroradiol* 1997;18: 1049–1056
49. Teresi L, Atkinson DJ, Chen DY, Fallon M, Patel S, Ko S, Cooney M, Bradley WG. **Diffusion-weighted Imaging of the C-spine: A new means of contrast for cord lesions.** 35th Annual Meeting of the ASNR 1997;270–270(Abstract)
50. Holder CA, Eastwood JD, Muthupillai R, Hudgins PA. **Diffusion-weighted MR imaging of the normal human spinal cord in Vivo.** 36th Annual Meeting of the ASNR 1998;190–190(Abstract)
51. Clark CA, Barker GJ, Tofts PS. **Magnetic Resonance Diffusion Imaging of the Human Cervical Spinal cord in vivo.** Seventh Scientific Meeting and Exhibition of the ISMRM 1998;(Abstract)
52. Enzmann DR, Rubin JB. **Cervical spine. MR imaging with a partial flip angle, gradient- refocused pulse sequence. Part I. General considerations and disk disease.** *Radiology* 1988;166: 467–472
53. Enzmann DR, Rubin JB. **Cervical spine. MR imaging with a partial flip angle, gradient- refocused pulse sequence. Part II. Spinal cord disease.** *Radiology* 1988;166:473–478

54. Hedberg MC, Drayer BP, Flom RA, Hodak JA, Bird CR. **Gradient echo (GRASS) MR imaging in cervical radiculopathy.** *AJR Am J Roentgenol* 1988;150:683–689
55. Kulkarni MV, Narayana PA, McArdle CB, Yeakley JW, Campagna NF, Wehrli FW. **Cervical spine MR imaging using multislice gradient echo imaging: comparison with cardiac gated spin echo.** *Magn Reson Imaging* 1988;6:517–525
56. Tsuruda JS, Norman D, Dillon W, Newton TH, Mills DG. **Three-dimensional gradient-recalled MR imaging as a screening tool for the diagnosis of cervical radiculopathy.** *AJNR Am J Neuroradiol* 1989;10:1263–1271
57. Russell EJ. **Cervical disk disease.** *Radiology* 1990;177:313–325
58. Tsuruda JS, Norman D, Dillon W, Newton TH, Mills DG. **Three-dimensional gradient-recalled MR imaging as a screening tool for the diagnosis of cervical radiculopathy.** *AJNR Am J Roentgenol* 1990;154:375–383
59. Carlson J, Crooks L, Ortendahl D, Kramer DM, Kaufman L. **Signal-to-noise ratio and section thickness in two-dimensional versus three-dimensional Fourier transform MR imaging.** *Radiology* 1988;166:266–270
60. Frahm J, Haase A, Matthaei D. **Rapid three-dimensional MR imaging using the FLASH technique.** *J Comput Assist Tomogr* 1986;10:363–368
61. Haacke EM, Tkach JA, Parrish TB. **Reduction of T2* dephasing in gradient field-echo imaging.** *Radiology* 1989;170:457–462
62. Wolff SD, Balaban RS. **Magnetization transfer contrast (MTC) and tissue water proton relaxation in vivo.** *Magn Reson Med* 1989;10:135–144
63. Wolff SD, Balaban RS. **Magnetization transfer imaging: practical aspects and clinical applications.** *Radiology* 1994;192:593–599
64. Wolff SD, Eng J, Balaban RS. **Magnetization transfer contrast: method for improving contrast in gradient-recalled-echo images.** *Radiology* 1991;179:133–137
65. Edelman RR, Ahn SS, Chien D, Li W, Goldmann A, Mantello M, Kramer J, Kleefield J. **Improved time-of-flight MR angiography of the brain with magnetization transfer contrast.** *Radiology* 1992;184:395–399
66. Pike GB, Hu BS, Glover GH, Enzmann DR. **Magnetization transfer time-of-flight magnetic resonance angiography.** *Magn Reson Med* 1992;25:372–379
67. Lin W, Tkach JA, Haacke EM, Masaryk TJ. **Intracranial MR angiography: application of magnetization transfer contrast and fat saturation to short gradient-echo, velocity- compensated sequences.** *Radiology* 1993;186:753–761
68. Finelli DA, Hurst GC, Gullapali RP, Bellon EM. **Improved contrast of enhancing brain lesions on postgadolinium, T1-weighted spin-echo images with use of magnetization transfer.** *Radiology* 1994;190:553–559
69. Elster AD, Mathews VP, King JC, Hamilton CA. **Improved detection of gadolinium enhancement using magnetization transfer imaging.** *Neuroimaging Clin N Am* 1994;4:185–192
70. Finelli DA. **Magnetization transfer in neuroimaging.** *Magn Reson Imaging Clin N Am* 1998;6:31–52
71. Melhem ER, Benson ML, Beauchamp NJ, Lee RR. **Cervical spondylosis: three-dimensional gradient-echo MR with magnetization transfer.** *AJNR Am J Neuroradiol* 1996;17:705–711
72. Tsuruda JS, Remley K. **Effects of magnetic susceptibility artifacts and motion in evaluating the cervical neural foramina on 3DFT gradient-echo MR imaging.** *AJNR Am J Neuroradiol* 1991;12:237–241
73. Haacke EM, Wielopolski PA, Tkach JA, Modic MT. **Steady–state free precession imaging in the presence of motion: application for improved visualization of the cerebrospinal fluid.** *Radiology* 1990;175:545–552
74. Zur Y, Wood ML, Neuringer LJ. **Motion-insensitive, steady-state free precession imaging.** *Magn Reson Med* 1990;16:444–459
75. Casselman JW, Kuhweide R, Deimling M, Ampe W, Dehaene I, Meeus L. **Constructive interference in steady state-3DFT MR imaging of the inner ear and cerebellopontine angle.** *AJNR Am J Neuroradiol* 1993;14:47–57
76. Georgy BA, Hesselink JR, Joseph PH. **3D CISS in MR imaging of the Cervical Spine.** 36th Annual Meeting of the ASNR 1998; 198–198(Abstract)
77. Gasparotti R, Ferraresi S, Pinelli L, Crispino M, Pavia M, Bonetti M, Garozzo D, Manara O, Chiesa A. **Three-dimensional MR myelography of traumatic injuries of the brachial plexus.** *AJNR Am J Neuroradiol* 1997;18:1733–1742
78. Zisch RJ, Hollenbach HP, Artmann W. **Lumbar myelography with three-dimensional MR imaging.** *J Magn Reson Imaging* 1992;2:731–734
79. VanDyke CW, Modic MT, Beale SM, Amartur S, Ross JS. **3D MR myelography.** *J Comput Assist Tomogr* 1992;16:497–500
80. Duerk JL, Lewin JS, Wendt M, Petersilge C. **Remember true FISP? A high SNR, near 1-second imaging method for T2-like contrast in interventional MRI at .2 T.** *J Magn Reson Imaging* 1998;8:203–208
81. Baur A, Stabler A, Bruning R, Bartl R, Krodel A, Reiser M, Deimling M. **Diffusion-weighted MR imaging of bone marrow: differentiation of benign versus pathologic compression fractures.** *Radiology* 1998;207:349–356
82. Le Bihan DJ. **Differentiation of benign versus pathologic compression fractures with diffusion-weighted MR imaging: a closer step toward the "holy grail" of tissue characterization?** *Radiology* 1998;207:305–307